ADVANCED FUNCTIONAL MATERIALS
www.afm-journal.de

Graphene-Enhanced 3D Chemical Mapping of Biological Specimens at Near-Atomic Resolution

Vahid R. Adineh, Changxi Zheng, Qianhui Zhang, Ross K. W. Marceau, Boyin Liu, Yu Chen, Kae J. Si, Matthew Weyland, Tony Velkov, Wenlong Cheng, Jian Li, and Jing Fu**

The direct imaging of individual atoms within the cellular context holds great potential for understanding the fundamental physical and chemical processes in organisms. Here, a novel approach for imaging of electrically insulated biological cells by introducing a graphene encapsulation approach to "disguise" the low-conductivity barrier is reported. Upon successful coating using a water-membrane-based protocol, the electrical properties of the graphene enable voltage pulsing field evaporation for atom probe tomography (APT). Low conductive specimens prepared from both Au nanoparticles and antibiotic-resistant bacterial cells have been tested. For the first time, a significant graphene-enhanced APT mass resolving power is also observed confirming the improved compositional accuracy of the 3D data. The introduction of 2D materials encapsulation lays the foundation for a breakthrough direction in specimen preparation from nanomembrane and nanoscale biological architectures for subsequent 3D near-atomic characterization.

1. Introduction

Knowledge acquired by various high-resolution imaging techniques including (cryo-)electron microscopy, confocal imaging, and secondary ion mass spectrometry (SIMS) has contributed to a fundamental understanding of cell biology as well as the engineered development of biomimetic materials with new physical and chemical properties.[1–8] Atom probe tomography (APT), the only technique offering 3D chemical measurements with near atomic resolution, has recently demonstrated its unique capability as a biological imaging tool to mammalian[9] and bacterial cells.[10]

However, the broader application of APT to the field is largely limited by the challenges in the sample preparation and the nonconductivity of biological specimens. A requirement of APT experiments is that the specimen material must be shaped into a sharp needle, typically with a tip radius less than 75 nm. By applying a positive voltage to the specimen under ultrahigh vacuum and cryogenic conditions, this tip geometry allows the generation of the sufficient electric field intensity to cause field ionization and evaporation of surface atoms. Controlled voltage pulsing allows the evaporation of individual and molecular ions that eventually reach a position sensitive detector. The impact positions and sequence of hits are employed to reconstruct their original position within the specimen and the time of flight is utilized to determine the atomic species.[11,12] In order to maintain a field density

V. R. Adineh, B. Liu, J. Fu
Department of Mechanical and Aerospace Engineering
Monash University
Clayton, VIC 3800, Australia
E-mail: jing.fu@monash.edu
C. Zheng, Q. Zhang
Department of Civil Engineering
Monash University
Clayton, VIC 3800, Australia
E-mail: changxi.zheng@monash.edu
R. K. W. Marceau
Institute for Frontier Materials
Deakin University
Geelong, VIC 3216, Australia
Y. Chen, M. Weyland
Monash Centre for Electron Microscopy
Monash University
Clayton, VIC 3800, Australia
M. Weyland
Department of Materials Science and Engineering
Monash University
Clayton, VIC 3800, Australia
K. J. Si, W. Cheng
Department of Chemical Engineering
Monash University
Clayton, VIC 3800, Australia
T. Velkov
Department of Pharmacology & Therapeutics
School of Biomedical Sciences
Faculty of Medicine
Dentistry and Health Sciences
The University of Melbourne
Parkville, VIC 3010, Australia
J. Li
Monash Biomedicine Discovery Institute
Department of Microbiology
Monash University
Clayton, VIC 3800, Australia
J. Fu
ARC Centre of Excellence for Advanced Molecular Imaging
Monash University
Clayton, VIC 3800, Australia

The ORCID identification number(s) for the author(s) of this article can be found under https://doi.org/10.1002/adfm.201801439.

DOI: 10.1002/adfm.201801439

sufficient for field evaporation, specimens need to be conductive to avoid charging effect. However, for organic and insulated materials such as biological cells, this imposes a major obstacle. Application of APT to imaging insulating materials has been enabled by achieving evaporation not by direct high-voltage pulsing, but by thermally driven evaporation using high-power, high-frequency laser pulsing.[13–15] Organic materials, however, are more sensitive to the application of a laser due to the possibility of thermally induced phase transition of the constituent molecules during the field evaporation process.[16] In previous studies, it has been demonstrated that a thin layer of conductive metal coated on an APT specimen can help fulfil the required voltage distribution for field evaporation of nonconductive materials.[10,17] This physical vapor deposition (PVD) based approach, however, also demonstrated limitations to achieve ultrathin coating of high-aspect ratio geometries, i.e., tip specimens for APT.[10,17] Figure S1a,b (Section S1, Supporting Information) presents an example of APT specimen prepared from resin-embedded bacterial cells with the previously devised PVD protocol. Improved mass resolving power (MRP) and specimen yield by tuning the conductive coatings have also been reported in the literature.[18–21] Tippey et al.[21] show that the MRP after coating exhibits a direct relationship with the thickness of the coating layer, suggesting an improved MRP if coating thickness is reduced. To this end, finding an ultrathin, highly conductive and strong coating layer may provide an optimal solution for imaging nonconductive materials.

In this study, we proposed and developed a technique of coating graphene films on delicate biological/organic APT specimens with high controllability, leading to sensitive and accurate chemical composition measurements. Recently, graphene has demonstrated an exceptional potential for coating applications,[22–24] including for nondestructive electron microscopy imaging and analysis of biological samples.[25] Uniform single-atom thickness, high density and other extraordinary physical properties (electrical and thermal conductivity, and mechanical properties)[26] should make graphene an ideal candidate for ultrathin coating high-aspect-ratio APT specimens. In our experiments, needle-shaped specimens suitable for APT are prepared from insulated and biological samples with site-specific, in situ focused ion beam (FIB) lift-out approach. Specific protocols are developed for coating with single-layer graphene and applied to low-conductivity specimens of resin-embedded Au nanoparticles (NPs) and individual bacterial cells, followed by 3D near-atomic resolution compositional mapping using pulsed-voltage APT.

2. Results and Discussion

2.1. Proposed Graphene Coating to Nonconductive Atom Probe Specimens

Figure 1 is a schematic of the proposed graphene encapsulation approach to achieve 3D near-atomic imaging of insulating materials with pulsed-voltage APT. The nonconductive specimens containing the regions of interest such as the cell envelope (Figure 1a) are prepared using a site-specific, in situ FIB lift-out technique.[10] In brief, subsamples (dissects) of a bacterial cell are further sectioned by FIB (keV, Ga^+), and sharpened into specimen needles (≈100 nm end-tip radius) having been mounted on W support posts after lift-out facilitated with an in situ micromanipulator. Figure 1b shows a scanning electron microscopy (SEM) image of an atom probe specimen containing the cellular dissect region of interest in the needle tip. The next critical step of the proposed approach is to position the monolayer or multilayer graphene film on the tip with minimal damage (Figure 1c). A tip specimen successfully coated multiple times with single graphene layers (Figure 1d) is then transferred to an APT instrument working in pulsed-voltage mode to generate a mass-to-charge-state ratio spectrum as shown in Figure 1e. Finally, using a back-projection reconstruction algorithm, a 3D map of the spatial distribution of atomic and molecular species can be constructed at near-atomic resolution (Figure 1e).

To achieve an optimal reconstruction of biological specimens, several coating characteristics need to be assessed: 1) minimal thickness of the coating layer is preferred to maintain the original specimen tip geometry and improve MRP.[21] 2) A continuous and uniform coating with negligible artefacts is required to avoid specimen failure during the APT experiment due to field-induced mechanical stresses.[10,17] 3) The coating needs to be chemically stable/inert and should not significantly weaken the mechanical strength of the specimen, especially considering that biological samples are typically fragile and temperature sensitive.

2.2. Electron Microscopy Characterization

Figure 2a illustrates the procedure proposed in the current study for coating APT tip specimens with a monolayer of graphene and further details are provided in the Experimental Section. Graphene is light-weight and hydrophobic due to its Van der Waals surface,[27] and as a result, graphene film has a tendency to maintain its 2D shape and float on the surface of liquids. This allows coating of APT specimens by control of the floating graphene film in direct contact with the target nanoscale specimen. With the support of a water membrane, the 2D graphene film starts to deform after contact with the nanoscale tip specimen, and continues to drape over the tip as the wire ring is lowered (Figure 2a). In the final stage, the movement of the wire ring is reversed lifting the water membrane until it is detached from the graphene-coated tip specimen.

An SEM image of a graphene-coated W tip specimen resulted from the water membrane based approach is presented in Figure 2b. Since the nominal thickness of graphene makes it relatively transparent to electrons, contrast of the graphene at the apex is low except for the regions where the graphene is folded (wrinkled).[28,29] An enlarged view of a folded region was acquired by scanning TEM (STEM) imaging in high-angle annular dark-field (HAADF) mode (Figure 2c) confirming the presence of graphene even 10 µm below specimen apex. Upon further HAADF STEM investigation of the region between the specimen apex and the folded regions, the formation of a continuous graphene film without detectable geometry change particularly at the apex is confirmed (Figure 2d,e). These results suggest that the proposed encapsulation approach based on a water membrane can provide a sufficiently gentle way to form

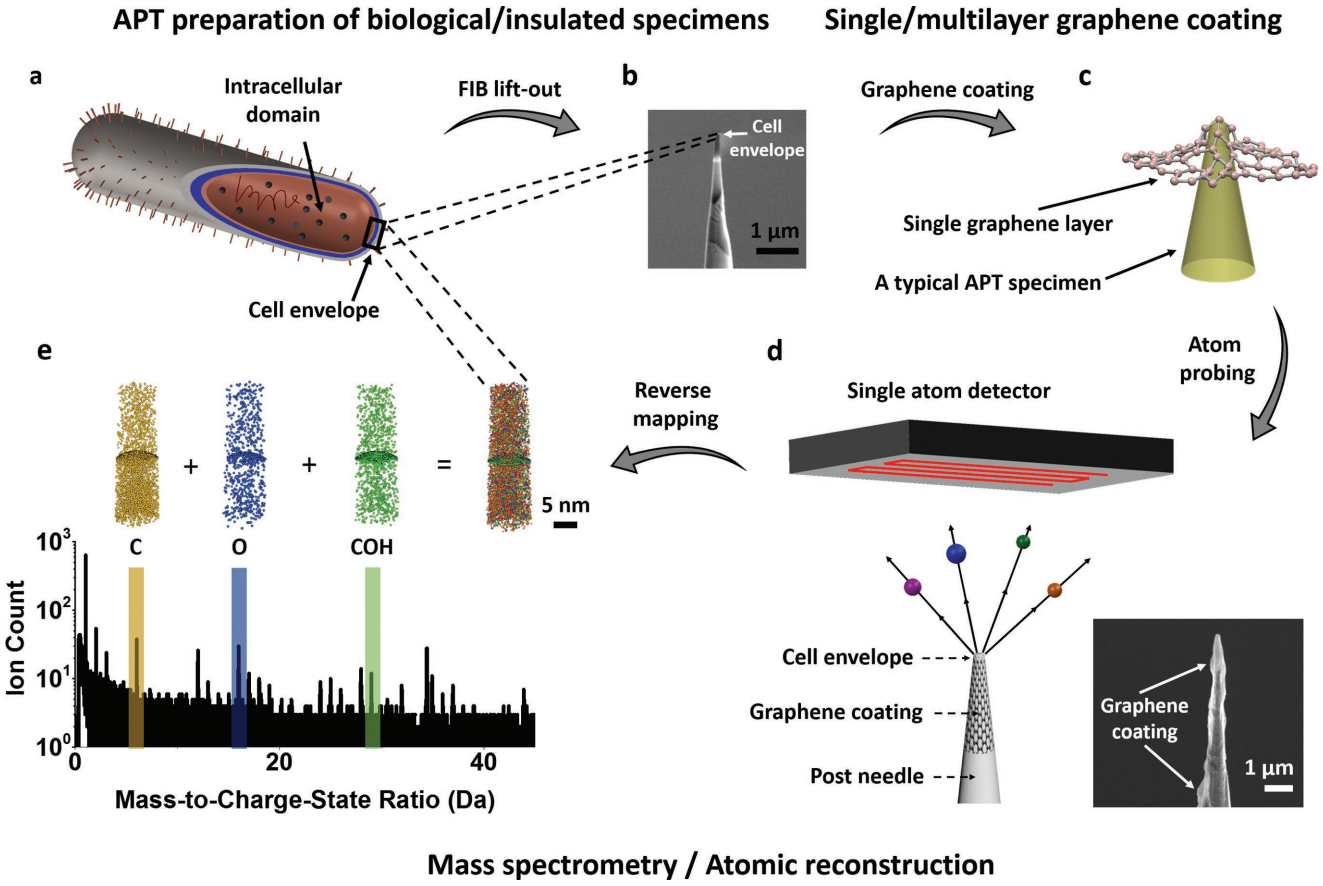

Figure 1. An overview of the proposed experimental design. a) Schematic image of a bacterial cell with cell envelope as the region of interest. b) A typical bacterial cell APT specimen containing the region of interest at the specimen apex, imaged by SEM. c) Schematic image of single-layer graphene encapsulation of an insulated APT tip specimen. d) Setup of pulsed-voltage atom probing, with an SEM image showing a typical APT specimen coated with single layers of graphene multiple times. e) A typical mass-to-charge-state ratio spectrum and 3D near-atomic reconstruction of volumes for these ratios.

a smooth, conductive layer on nanoscale APT specimens. It should be noted that encapsulation of van der Waals layered materials in air may trap contaminants such as hydrocarbon at the interface to increase the detectable thickness.[30] Similarly, variations of graphene thickness based on the TEM images in this study are also likely due to trapping of hydrocarbon.

Alternative approaches for coating of high-aspect-ratio nanoscale samples as previously reported remain incompatible for APT specimens prepared from biological and temperature sensitive materials due to the high temperatures or chemicals involved in those processes.[31–34] Comparison is provided with in situ FIB-SEM graphene coating approach and atomic layer deposition (ALD) method (Section S3, Supporting Information). Due to the exceptional mechanical strength and flexibility of graphene,[35,36] sharp atom probe specimens can be coated using graphene which adheres almost completely to the tip geometry to form a conductive layer. Although possible damage and artefacts due to the graphene encapsulation cannot be precluded (Section S2, Supporting Information), overall coating success rate is reasonably high (above 60%) for the organic specimens in this study. Shown in **Figure 3**a–f are further applications of graphene encapsulation to insulated APT specimens prepared from both bacterial cells and resin-embedded Au NPs. Figure 3b,e shows typical specimens after single layer graphene coating. Multilayer graphene coatings can also be formed by repeating the single layer coating process, as shown in Figure 3c,f.

To investigate the coupling conductivity of graphene with nanostructures, a device consisting of a chemically assembled Au nanoparticle membrane has been fabricated for conductivity measurements. Shown in Figure 3g is a schematic of the device with a layer of graphene on top of the Au particle membrane, and for comparison Figure 3h shows a TEM image of a typical resin-embedded Au NPs APT specimen without coating. Further details about the device including the wiring for conductivity measurement are included in Section S4 (Supporting Information). The target Au particles are assembled with a polymer-assisted bottom-up method, and each particle is surrounded by a layer of nonconductive polystyrene[37] (Figure 3g), representing Au NPs in the resin-embedded APT specimen (Figure 3h). When the voltage is at 0.5 V, the current in the membrane is below a nanoampere (blue curve in Figure 3i). With the graphene layer on top, the current increases beyond a micro-ampere, as demonstrated by the red curve in Figure 3i. This result confirms that for graphene in contact with individual nanostructures, charge can flow freely on the surface which is desirable for efficient field evaporation.

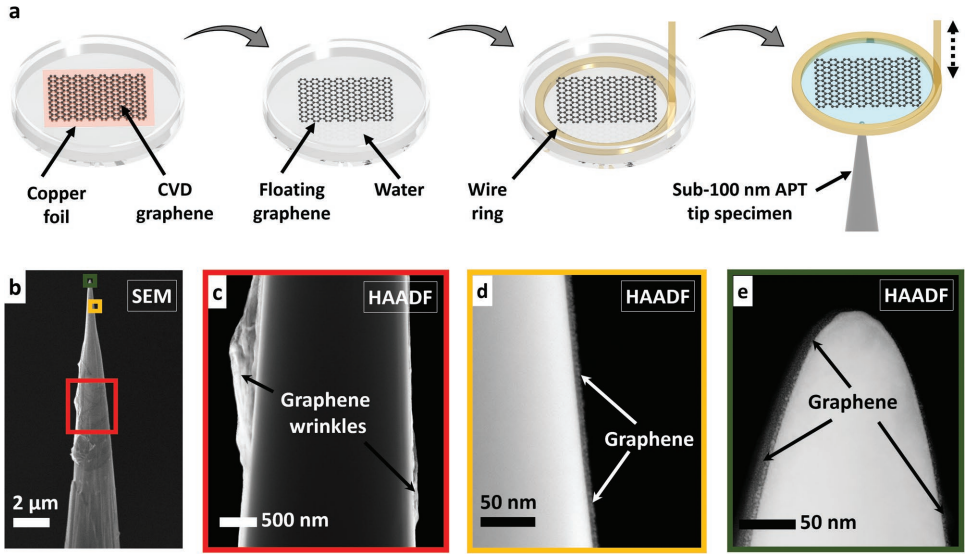

Figure 2. Detailed steps of graphene encapsulation and investigation with electron microscopy. a) The steps of graphene coating include: etching Cu foil to separate chemical vapor deposited graphene using ammonia persulphate solution (APS); replacement of APS with deionized water after Cu etching; retrieval of the graphene layer using a nichrome wire ring; and coating the APT specimen by lowering the graphene film on top of the specimen. b) SEM image of a typical graphene-coated W tip specimen, with the selected regions for STEM imaging. c) HAADF STEM image of the graphene wrinkles from the red box in b) showing wrinkles formed by the covering graphene. d) HAADF STEM image of the tip region a few micrometers below the apex (represented by yellow box in (b)). e) HAADF STEM image of the specimen apex (represented by green box in (b)).

2.3. Atom Probe Tomography of Resin-Embedded Au NPs with Graphene Encapsulation

To explore the feasibility of the proposed graphene coating approach to facilitate APT imaging of insulated materials, Au NPs were chosen as a test specimen due to the ease of verification of geometry and composition. **Figure 4**a shows an SEM image of a typical resin-embedded Au NPs APT specimen after graphene coating, and the corresponding high-magnification bright-field (BF) STEM image of the specimen apex shown in Figure 4b confirms no visible damage on the specimen tip after coating. This specimen was then transferred into the atom probe instrument to acquire data in pulsed-voltage mode, where the 3D atom map reconstructed from the acquired mass spectrum are presented in Figure 4c,d, respectively.

As expected, the mass spectrum in Figure 4d contains Au (in this case, the 2nd charge state isotope at 98.5 Da) together with other peaks, collectively from the resin and graphene, as well as Ga peaks due to ion beam implantation. Details of the mass spectrum and 3D atom maps of resin and Ga species are provided in Section S5 (Supporting Information). A notable finding from the acquired mass spectrum is an improved MRP from graphene-coated specimens compared to the metal coated control specimens.[17] Figure 4e compares the shapes of the mass peaks of Au^{2+} acquired from both graphene coating and Ag sputter coating[17] in a limited mass spectrum range (97–100 Da). A remarkable improvement in the shape of the mass peak is observed for the graphene-coated specimen, and as a result a higher MRP of 955 (mass-to-charge value of a peak divided by the peak width at half the maximum (FWHM)) compared to that of the Ag sputter-coated specimen[17] (MRP = 492), which demonstrates significantly improved mass resolution using graphene (see the Experimental Section for further discussions on MRP definition and comparison). It should be noted that the experimental conditions remained the same for comparing graphene and metal coating approaches (see Figure S7e in the Supporting Information). The observation of higher MRP, equating to higher compositional accuracy, is expected as a result from the increased uniformity of the local field distribution and evaporation potential across the graphene-coated apex during probing (see computational studies in Section S6 of the Supporting Information).

2.4. Graphene-Enabled APT Imaging of Biological Cells

APT tip specimens containing the cell envelope region of a dehydrated bacterial cell were also coated by single graphene layers a multiple number of times, followed by pulsed-voltage APT. These specimens were prepared from resistant strains of *Acinetobacter baumannii* (ATCC 19606 R) and were prepared in a similar fashion to a conventional lift-out procedure[11,38,39] (see the Experimental Section for further information). After successful graphene coating based on the water-membrane-assisted protocol, the coated bacterial APT specimens, as well as uncoated controls, were subsequently run in the atom probe in pulsed-voltage mode. Successful 3D atom maps of various ionic species acquired from graphene-coated specimen are shown in **Figure 5**a,b. All the uncoated control specimens failed during probing. Detailed mass spectra acquired from two graphene-coated bacterial specimens and further discussion are presented in Section S7 (Supporting Information), along with 3D atom maps (Sections S8 and S9 and Figures S11 and S12, Supporting Information).

In the mass spectra acquired by APT from bacterial specimens, distinct peaks from H, C, N, O and associated molecular

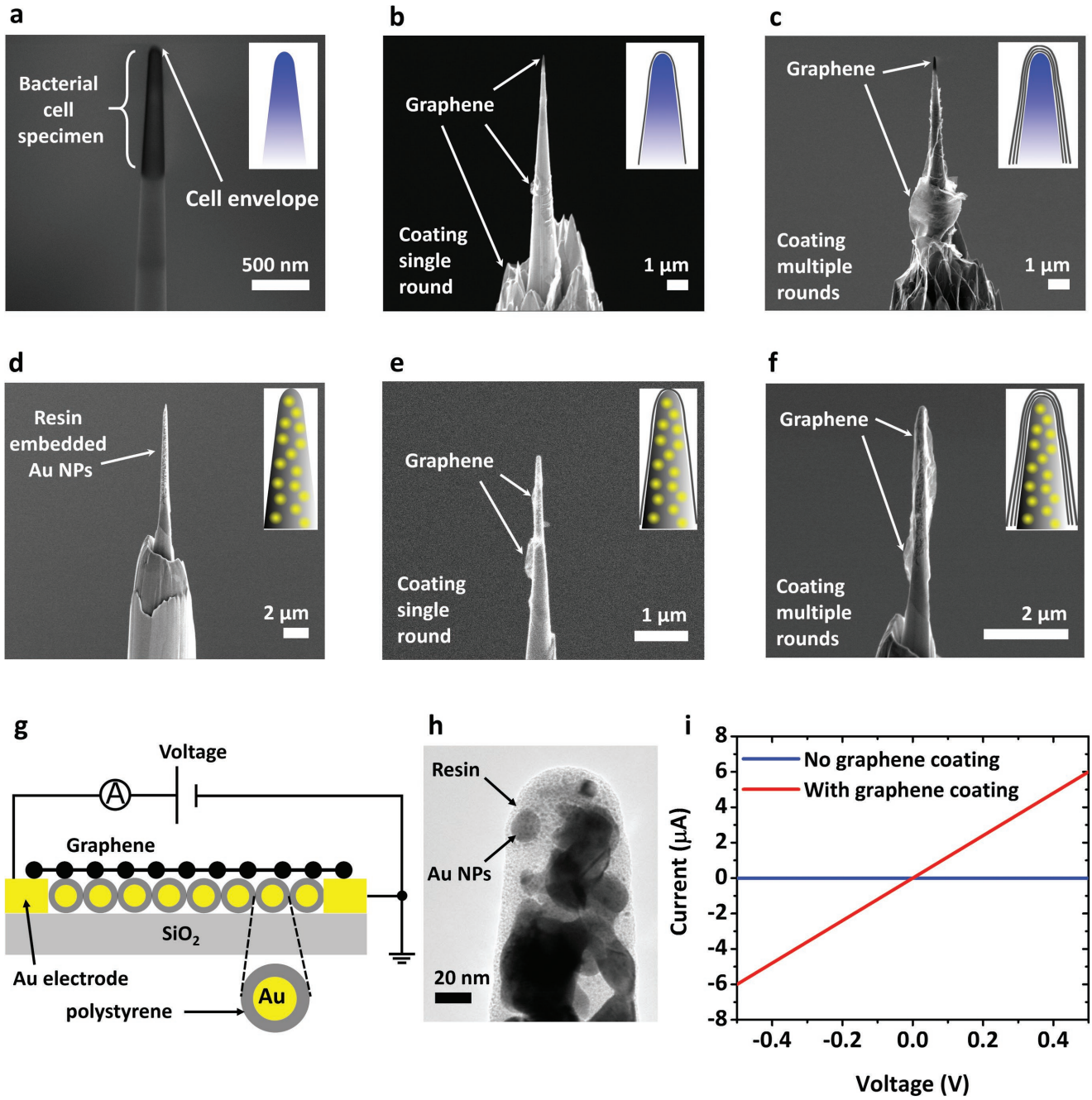

Figure 3. Controllable graphene encapsulation on various specimens to enhance the conductivity. SEM images of: a) A bacterial cell APT specimen without coating; b) a bacterial cell APT specimen coated with a single graphene layer; c) a bacterial cell APT specimen coated multiple times with single graphene layers; d) a typical resin-embedded Au NPs APT specimen without coating; e) a typical resin-embedded Au NPs APT specimen coated with a single graphene layer; and f) a typical resin-embedded Au NPs APT specimen coated multiple times with single graphene layers. g) Schematic of a graphene-coated Au nanoparticle membrane device. h) TEM image of a typical resin-embedded Au NPs APT specimen. i) The current versus voltage curves measured by the device before and after graphene coating, respectively.

forms such as C_2H_3 (27 Da), CO (28 Da), COH (29 Da), OH_3 (19 Da), and CO_2 (44 Da) have been identified (see Figure S10 of the Supporting Information for detailed spectra). For atomic and molecular C, as well as complex molecular ions, it should be noted that partial contribution from graphene cannot be excluded. Peaks from Ga^+ and Ga^{2+} (69 and 34.5 Da) are also present, which are due to Ga implantation during FIB milling (<3.2 at% in the first specimen and <0.3 at% in the repeat). In one of the mass spectra acquired, small peaks (<0.5 at%) pertaining to Pt (97, 97.5, 98, and 99 Da) have been observed, which are likely due to remnants of Pt protective layer applied during FIB lift-out specimen preparation. The 3D atom maps of Pt and Ga suggest that penetration of Ga ions into the cellular APT specimen is higher in the regions with less protective

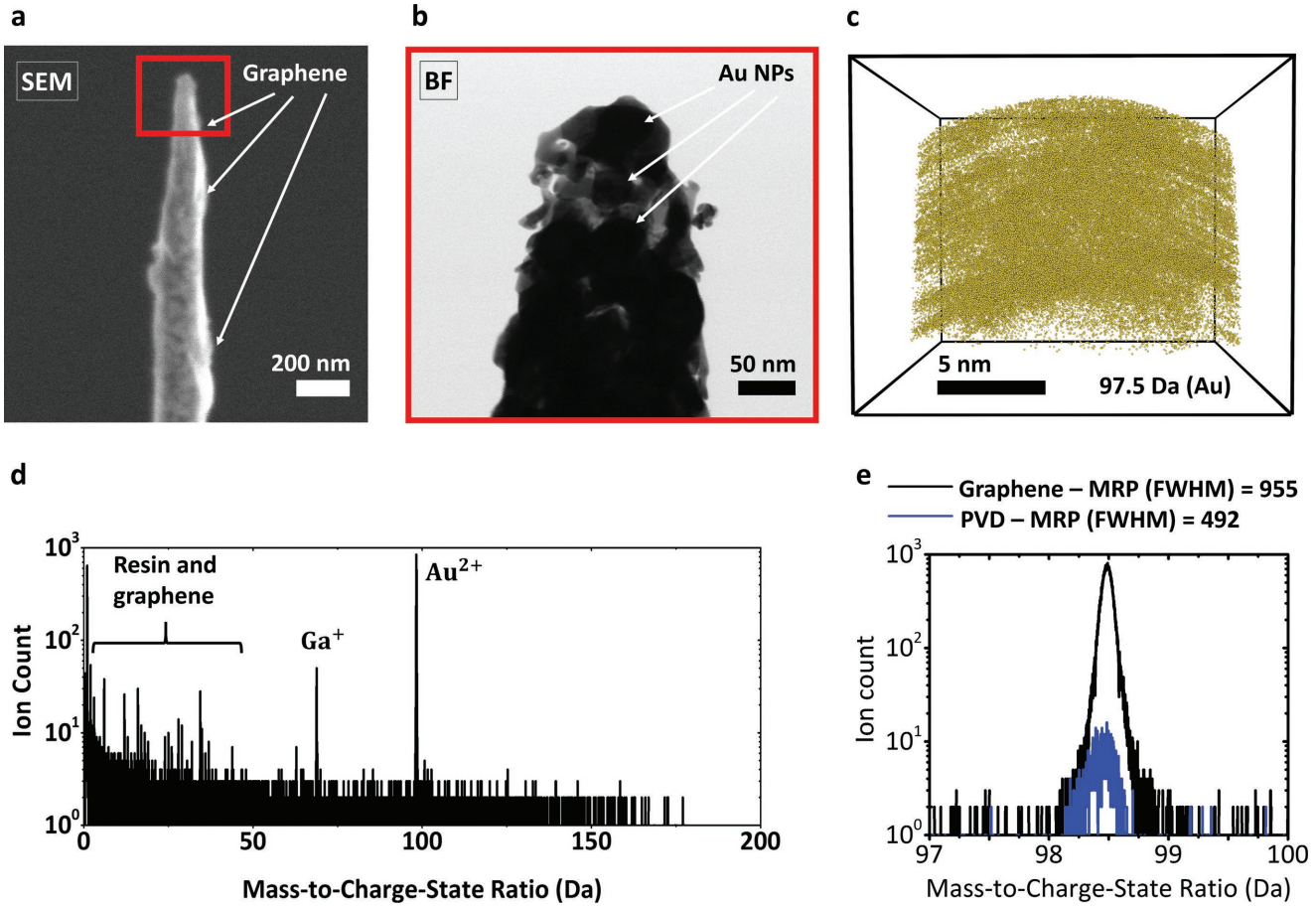

Figure 4. APT of Au nanoparticles with graphene coating. a) SEM image of a typical resin-embedded Au NPs APT specimen after graphene coating. b) High magnification BF STEM image of the specimen apex from the red box in a) confirms no visible damage on the specimen apex after graphene coating. c) 3D near-atomic chemical mapping of a typical resin-embedded Au NPs APT specimen along with corresponding; d) mass-to-charge-state ratio spectrum. e) Comparison of peaks of the second charge state of Au acquired from graphene-coated and PVD Ag sputter-coated[17] specimens of resin-embedded Au NPs, together with the associated MRP values. The experimental conditions are the same in the both spectrums; voltage (*V*) of 4 kV, and ion flight path length (*L*) of 382 mm.

Pt layer (see Section S8 and Figure S11 of the Supporting Information).

The reconstructed 3D nanostructural mapping of the cell envelope enabled by graphene encapsulation is shown in Figure 5a. Similar patterns of atomic distribution are also observed in a repeat (cell envelope) sample (see Section S9 in the Supporting Information), including small clusters from the 28 Da peak (CO) of ≈1 nm in size (Figure 5b). This is also similar to previously reported APT data,[10] where molecular fragments of phosphocholine are absent, suggesting loss or damage of the lipid layers of resistant bacterial strains.[40] On a final note, the physical mechanisms involved in field-evaporation-based, APT imaging of cellular specimens using the current graphene coating approach was investigated by comparison of the average operating voltage range during APT experiments with that for Ag sputter-coated cellular APT specimens.[10] Figure 5c shows the former allows a lower operating voltage range than the latter, for a similar specimen tip radius prior to coating. Lower voltage for the graphene-coated specimens consequently led to lower field-induced mechanical stresses, and enabled a higher success rate of data acquisition (average success rate of 15%, i.e., 3 successful runs out of 20 experiments) as compared to the samples sputter-coated with Ag by PVD (average success rate of 5%[10,17]).

Figure S14 (Supporting Information) shows further application of the developed APT graphene coating method for sandwiching a water nanomembrane (WNM) onto the apex of an APT specimen. After multiple coatings to a W APT specimen with monolayer graphene films, a pure water membrane was trapped at the specimen apex due to the excellent impermeability of graphene (see Section S11 of the Supporting Information). The features inside the WNM are probably the nanobubbles which will be interesting to future explorations.

3. Conclusion

In this study, a novel approach to explore the structure and chemistry of biological specimens at near atomic resolution is explored. It has been demonstrated that imaging of low-conductivity specimens with pulsed-voltage APT can be achieved by applying graphene encapsulation. The

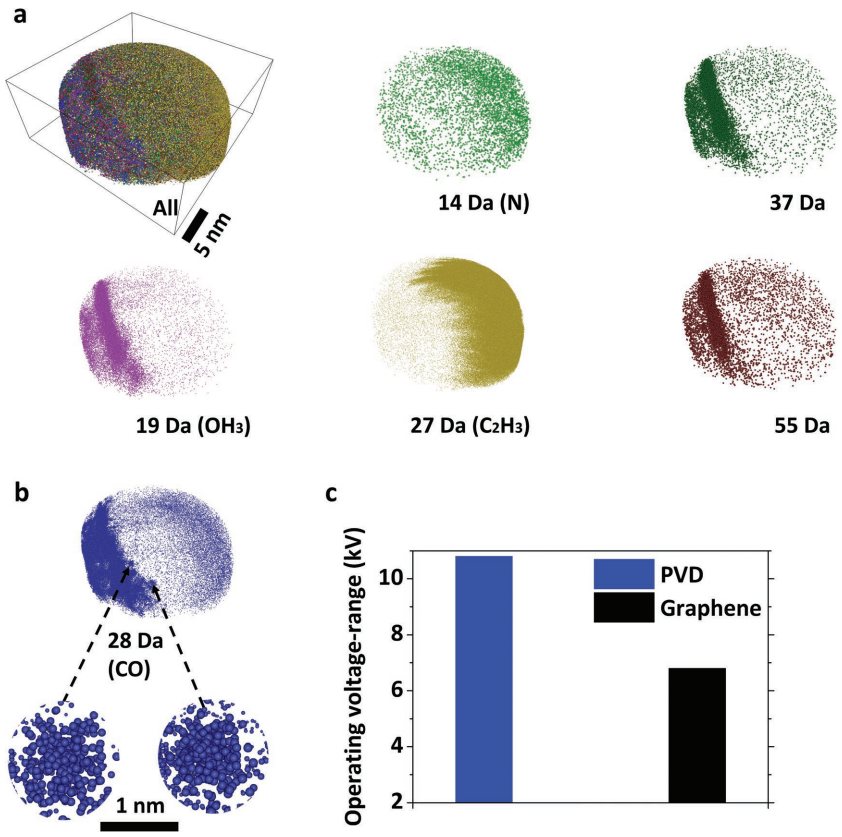

Figure 5. APT of bacterial cell envelope with graphene coating. a) Reconstructed 3D volumes of cell envelope together with reconstructed 3D maps of selected ionic species. b) 3D map of CO species that contains 1 nm clusters. c) Operating voltage range of graphene-coated (this study) and Ag sputter-coated cellular APT specimens.[10,17]

water-membrane-assisted graphene coating technique demonstrates minimal damage when applied to APT specimens prepared from different types of materials such as metallic, polymeric and biological specimens. Due to its single-atom thickness and extraordinary conductivity, the addition of a graphene layer enables formation of strong electrical field at the apex of the specimen during APT field evaporation. Improved compositional accuracy and specimen yield are demonstrated from the MRP of the acquired mass spectra, as well as a lowered operating voltage range. The proposed encapsulation approach with 2D graphene material for APT specimens provides a novel route toward imaging low-conductivity material at near atomic resolution, and lays a solid foundation for future research requiring interrogation of intracellular chemistry.

4. Experimental Section

Graphene Coating Technique: To coat the tip specimens with graphene, large-area single/monolayer graphene films were grown on copper foil by chemical vapor deposition. The copper foil was etched away by 0.1 M ammonium persulfate solution (APS). After etching, the APS solution was removed by a syringe until there was a thin layer of liquid to avoid graphene touching the bottom of container. Deionized (DI) water (Milli-Q water) was then injected into the container. The removal and injection procedures were repeated at least four times to replace the APS with DI water. The graphene layer was then floating on top of DI water and a nichrome wire ring was employed to retrieve the graphene film from the DI water in the petri dish. A water membrane is typically formed inside the wire ring due to surface tension, and its thickness is determined by the diameter of the wire. In this study a nichrome wire with diameter 0.25 mm was utilized to form an ultrathin water membrane. To carry out the coating, the wire ring was placed above an APT specimen and moved down slowly toward the specimen. Once the graphene was picked up by the APT specimen, the motion of the wire ring was reversed to retreat from the APT specimen. SEM examination of the APT specimen was subsequently carried out to ensure that the coating was successful and the specimen was not damaged. It is possible that defects contained in the graphene layer affected the coating quality. Therefore samples were routinely coated for two or three times to mitigate the effects of defect. Usually after two or three rounds, the graphene layers could be clearly observed to cover the tip with SEM, and excessive coating rounds have been avoided to lower the risk of damaging the delicate biological tips.

Au NPs Preparing and Resin Embedding: Gold chloride trihydrate ($HAuCl_4 \cdot 3H_2O$, ≥99.9%), hexadecyltrimethylammonium bromide (CTAB), cetyltrimethylammonium chloride solution (CTAC, 25 wt% in water), silver nitrate ($AgNO_3$), sodium borohydride ($NABH_4$), and L-ascorbic acid (AA) were purchased from Sigma Aldrich and without further purification were used to synthesize the Au NPs based on a repeated seeded growth approach,[41] as detailed elsewhere.[42] After preparing a high concentration Au NPs solution, it was spun down at 14 500 rpm for 10 min and rinsed with Milli-Q water three times in a 1.5 mL Eppendorf tube. Resin embedding of Au NPs was carried out based on a protocol reported at our previous work.[17] The NPs were dissolved in 100% acetone for 10 min, 2 times followed by infiltrating with 100% EPON 2 times and the infiltration process was accelerated in BioWave (Ted Pella Inc, USA). Polymerization of the resin was carried out overnight (24 h) in an oven set at 60 °C.[17]

Bacterial Cell Culture: The same polymyxin resistant *Acinetobacter baumannii* strains (ATCC 19606 R) as utilized in our previous study[10] were used in this work for APT cellular specimen preparation. The colony was first inoculated into cation-adjusted Mueller-Hinton Broth (CAMHB), and incubated overnight for 18 h in a shaking batch. The log-phase cultures were prepared by inoculating 1:100 of the overnight culture into CAMHB, and incubated for another 3.5 h. Moreover, using Milli-Q water and 0.22 µm syringe filter, sterile 1 mg mL^{-1} solution of polymyxin B sulfate was prepared. The cells were washed 3 times in phosphate buffered saline (PBS), and fixation was performed with 4% paraformaldehyde (PFA) in PBS for 20 min. At the final step, the specimens were washed two times with PBS, and were added as a suspension (10 µL) onto the silicon nitride membrane window on a silicon wafer (Ted Pella Inc., CA, USA). The specimens were allowed to air dry overnight in a biosafety cabinet. Further details are provided elsewhere.[10]

Electron Microscopy Characterizations: TEM sample preparation from APT samples was performed using FIB lift-out method. A FIB-SEM instrument (Quanta 3D FEG, FEI Company) equipped with a chamber-installed micromanipulator (MM3A-EM, Kleindiek Nanotechnik GmbH) was utilized to cut, transfer and mount the graphene-coated APT specimens on to TEM half-grids. Further details of TEM specimen preparation for imaging of the coated APT tips have been reported elsewhere.[17] Detailed studies of morphology and elemental analysis

were carried by STEM and energy-dispersive X-ray spectroscopy, conducted on a transmission electron microscope (Tecnai G2 F20 S-TWIN, FEI/Thermo Fisher Scientific, OR, USA) operating at 200 kV.

APT Specimen Preparation and Run Parameters: Specimens for APT analysis as well as PVD and chemical vapor deposition trial coating experiments were prepared based on the conventional FIB lift-out technique.[11,38,39] A FIB-SEM instrument (Quanta 3D FEG, FEI/Thermo Fisher Scientific, OR, USA) equipped with a chamber-installed micromanipulator (MM3A-EM, Kleindiek Nanotechnik GmbH) was utilized for the FIB lift-out APT specimen preparation. For all of the bulk samples, the three stages of APT specimen preparation' i.e., wedge preparation, wedge lift-out/attachment to the post needle, and annular milling for sharpening of the tips were utilized.[10] The difference between APT specimen preparation from the resin-embedded Au NPs and the dehydrated bacterial cells is that with the resin-embedded Au NPs, a long wedge was shared amongst various support post needles, while for the cellular specimens, a complete lift-out procedure was performed for each bacterial cell. Further details regarding APT sample preparation can be found in the previous studies.[10,17] Additional details of APT specimen preparation from resin-embedded bacterial cells are provided in Supporting Information (Section S12, Supporting Information).

APT experiments were conducted using a LEAP 4000 HR instrument (CAMECA Instruments, USA) operating in voltage mode under ultrahigh vacuum ($<1 \times 10^{-11}$ Torr). The operational parameters were set as following: set-point temperature of 60 K, pulse fraction of 20%, pulse repetition rate of 200 kHz and detection rate of 0.005 atoms per pulse.

Definition of MRP: MRP is a key characteristic of a time-of-flight (TOF) mass spectrometer, and it demonstrates the ability of the instrument to characterize two ions that are close in mass. The MRP at FWHM is $(m/n)/\Delta(m/n)$, which is mass-to-charge (m/n) value of a peak divided by the peak width at half the maximum of the peak. This value is therefore dimensionless.[14] In an APT instrument, however, the MRP depends on m/n, and also the operating conditions such as voltage (V) and ion flight path length (L).[14] Thus, to compare the MRP from one APT experiment to next, the same m/n value at the same V and L should be utilized.[14] In this work, to compare the MRP values of PVD Ag sputter-coated resin-embedded Au NPs specimens with the graphene-coated specimens, $m/n = 98.5$, $V = 4$ kV, and $L = 382$ mm were utilized in both cases.

APT Reconstruction and 3D Visualization: Tomographic reconstructions of the APT data were performed with the IVAS 3.6.12 software instrument (CAMECA Instruments, USA) followed by transfer of the coordinate data (x, y, and z) for 3D visualization using FEI Avizo 9.1 software (FEI/Thermo Fisher Scientific, OR, USA), and Blender (The Blender Foundation, www.blender.org).

Supporting Information

Supporting Information is available from the Wiley Online Library or from the author.

Acknowledgements

V.R.A. and C.Z. contributed equally to this work. C.Z. thanks support from ARC DECRA (DE140101555). This study was partly funded by the Australian Research Council (DP180103955), the Australian National Health & Medical Research Council (APP1046561), Monash University Interdisciplinary Research (IDR) Seed Fund, and the Monash Centre for Atomically Thin Materials (MCATM) (for PhD top-up scholarship). This work was performed in part at the Melbourne Centre for Nanofabrication (MCN), Victorian Node of the Australian National Fabrication Facility (ANFF), Monash Centre for Electron Microscopy (MCEM) and the Advanced Characterisation Facility within the Institute for Frontier Materials (IFM) at Deakin University. J.L. and T.V. are supported by a research grant from the National Institute of Allergy and Infectious Diseases of the National Institutes of Health (R01 AI132154). The content is solely the responsibility of the authors and does not necessarily represent the official views of the National Institute of Allergy and Infectious Diseases or the National Institutes of Health. J.L. is an Australian NHMRC Senior Research Fellow. T.V. is an Australian NHMRC Industry Career Development Level 2 Research Fellow. This research used equipment funded by Australian Research Council (ARC) grants (LE0882821, LE110100223, and LE120100034). The authors would like to thank Drs Amelia Liu, Flame Burgmann, Jisheng Ma, and Peter Miller for their assistance during this study.

Conflict of Interest

The authors declare competing financial interests in the form of an Australian provisional patent (Application No: 2017902581).

Keywords

atom probe tomography, cellular imaging, graphene

Received: February 25, 2018
Revised: May 7, 2018
Published online: June 20, 2018

[1] J. Dubochet, M. Adrian, J. Chang, J. Homo, J. Lepault, A. McDowall, P. Schultz, *Q. Rev. Biophys.* **1988**, *21*, 129.
[2] M. Marko, C. Hsieh, W. Moberlychan, C. A. Mannella, J. Frank, *J. Microsc.* **2006**, *222*, 42.
[3] M. Marko, C. Hsieh, R. Schalek, J. Frank, C. Mannella, *Nat. Methods* **2007**, *4*, 215.
[4] *Nat. Methods* **2016**, *13*, 1.
[5] J. Frank, *Nat. Protoc.* **2017**, *12*, 209.
[6] J. S. Fletcher, J. C. Vickerman, N. Winograd, *Curr. Opin. Chem. Biol.* **2011**, *15*, 733.
[7] M. K. Passarelli, A. G. Ewing, N. Winograd, *Anal. Chem.* **2013**, *85*, 2231.
[8] L. J. Gamble, C. R. Anderton, *Microsc. Today* **2016**, *24*, 24.
[9] K. Narayan, T. J. Prosa, J. Fu, T. F. Kelly, S. Subramaniam, *J. Struct. Biol.* **2012**, *178*, 98.
[10] V. R. Adineh, R. K. Marceau, T. Velkov, J. Li, J. Fu, *Nano Lett.* **2016**, *16*, 7113.
[11] T. F. Kelly, M. K. Miller, *Rev. Sci. Instrum.* **2007**, *78*, 031101.
[12] M. K. Miller, *Atom Probe Tomography, Analysis at the Atomic Level*, Kluwer Academic/Plenum Publishers, New York **2000**.
[13] M. K. Miller, R. G. Forbes, *Atom-Probe Tomography: The Local Electrode Atom Probe*, Springer, New York **2014**.
[14] D. J. Larson, T. Prosa, R. Ulfig, B. Geiser, T. Kelly, *Local Electrode Atom Probe Tomography*, Springer, New York **2013**.
[15] B. Gault, M. P. Moody, J. M. Cairney, S. P. Ringer, *Atom Probe Microscopy*, Springer Science & Business Media, New York **2012**.
[16] T. F. Kelly, O. Nishikawa, J. A. Panitz, T. J. Prosa, *MRS Bull.* **2009**, *34*, 744.
[17] V. R. Adineh, R. K. W. Marceau, Y. Chen, K. J. Si, T. Velkov, W. Cheng, L. Jian, J. Fu, *Ultramicroscopy* **2017**, *181*, 150.
[18] G. Kellogg, *J. Appl. Phys.* **1982**, *53*, 6383.
[19] D. Larson, T. Prosa, J. Bunton, D. Olson, D. Lawrence, E. Oltman, S. Strennin, T. Kelly, *Microsc. Microanal.* **2013**, *19*, 994.
[20] J.-B. Seol, C.-M. Kwak, Y. T. Kim, C.-G. Park, *Appl. Surf. Sci.* **2016**, *368*, 368.
[21] K. Tippey, J. G. Brons, M. Kapoor, B. Fu, G. B. Thompson, *Thin Solid Films* **2014**, *551*, 32.
[22] A. Akturk, N. Goldsman, *J. Appl. Phys.* **2008**, *103*, 053702.

[23] A. K. Geim, K. S. Novoselov, *Nat. Mater.* **2007**, *6*, 183.
[24] K. S. Novoselov, A. K. Geim, S. V. Morozov, D. Jiang, Y. Zhang, S. V. Dubonos, I. V. Grigorieva, A. A. Firsov, *Science* **2004**, *306*, 666.
[25] J. B. Park, Y.-J. Kim, S.-M. Kim, J. M. Yoo, Y. Kim, R. Gorbachev, I. Barbolina, S. J. Kim, S. Kang, M.-H. Yoon, *2D Mater.* **2016**, *3*, 045004.
[26] K. S. Novoselov, V. I. Falko, L. Colombo, P. R. Gellert, M. G. Schwab, K. Kim, *Nature* **2012**, *490*, 192.
[27] Z. Li, Y. Wang, A. Kozbial, G. Shenoy, F. Zhou, R. McGinley, P. Ireland, B. Morganstein, A. Kunkel, S. P. Surwade, L. Li, H. Liu, *Nat. Mater.* **2013**, *12*, 925.
[28] N. R. Wilson, P. A. Pandey, R. Beanland, R. J. Young, I. A. Kinloch, L. Gong, Z. Liu, K. Suenaga, J. P. Rourke, S. J. York, J. Sloan, *ACS Nano* **2009**, *3*, 2547.
[29] J. M. Yuk, J. Park, P. Ercius, K. Kim, D. J. Hellebusch, M. F. Crommie, J. Y. Lee, A. Zettl, A. P. Alivisatos, *Science* **2012**, *336*, 61.
[30] S. J. Haigh, A. Gholinia, R. Jalil, S. Romani, L. Britnell, D. C. Elias, K. S. Novoselov, L. A. Ponomarenko, A. K. Geim, R. Gorbachev, *Nat. Mater.* **2012**, *11*, 764.
[31] Y. Wen, J. Chen, Y. Guo, B. Wu, G. Yu, Y. Liu, *Adv. Mater.* **2012**, *24*, 3482.
[32] M. Pacios, P. Hosseini, Y. Fan, Z. He, O. Krause, J. Hutchison, J. H. Warner, H. Bhaskaran, *Sci. Rep.* **2016**, *6*, 22700.
[33] M. Lanza, A. Bayerl, T. Gao, M. Porti, M. Nafria, G. Jing, Y. Zhang, Z. Liu, H. Duan, *Adv. Mater.* **2013**, *25*, 1440.
[34] W. Shim, K. A. Brown, X. Zhou, B. Rasin, X. Liao, C. A. Mirkin, *Proc. Natl. Acad. Sci. USA* **2012**, *109*, 18312.
[35] J.-H. Ahn, B. H. Hong, *Nat. Nanotechnol.* **2014**, *9*, 737.
[36] C. Lee, X. Wei, J. W. Kysar, J. Hone, *Science* **2008**, *321*, 385.
[37] K. J. Si, D. Sikdar, Y. Chen, F. Eftekhari, Z. Xu, Y. Tang, W. Xiong, P. Guo, S. Zhang, Y. Lu, Q. Bao, W. Zhu, M. Premaratne, W. Cheng, *ACS Nano* **2014**, *8*, 11086.
[38] M. K. Miller, K. F. Russell, G. B. Thompson, *Ultramicroscopy* **2005**, *102*, 287.
[39] K. Thompson, D. Lawrence, D. J. Larson, J. D. Olson, T. F. Kelly, B. Gorman, *Ultramicroscopy* **2007**, *107*, 131.
[40] J. H. Moffatt, M. Harper, P. Harrison, J. D. Hale, E. Vinogradov, T. Seemann, R. Henry, B. Crane, F. S. Michael, A. D. Cox, *Antimicrob. Agents Chemother.* **2010**, *54*, 4971.
[41] C. Ziegler, A. Eychmüller, *J. Phys. Chem. C* **2011**, *115*, 4502.
[42] K. J. Si, D. Sikdar, L. W. Yap, J. K. K. Foo, P. Guo, Q. Shi, M. Premaratne, W. Cheng, *Adv. Opt. Mater.* **2015**, *3*, 1710.